Clockwork Orangutan: microRNAs, thermoregulatory tradeoffs, and the evolution of brain size.

Bastian Fromm*, PhD

The Arctic University Museum of Norway

UiT- The Arctic University of Norway 9037

Tromsø, Norway

Thomas Sorger, PhD

Department of Biology

Roger Williams University

Bristol, Rhode Island 02809, USA

*** corresponding author**

SUMMARY

Hypotheses to account for the energy demand associated with the disproportionate increase in brain size in the human lineage have not considered thermoregulatory constraints. Unlike log-based specific metabolic rates (*sMR*s), the distribution of cellular *MR*s (*cMR*s) can be matched to relevant traits, like body temperature and the number of microRNA families (*mirFam*). We demonstrate that the *mirFam*-based *cMR*s of the four most thermogenic organs (kidney, heart, liver and brain) form a core with a joint *cMR* that scales as $M^{0.52}$, as predicted by a comprehensive biophysical model of thermoregulation in homeotherms. Across Euarchontoglires, core organs do not evolve independently: while organ sizes depend on body size, organ *cMR*s depend on the core *cMR*. Consequently, brain and liver *cMR*s are strictly anti-correlated, echoing the expensive tissue hypothesis. We propose a positive feedback relationship between larger brain size and greater reliability of the energy supply, on the one hand, and decreasing reliance on liver gluconeogenesis on the other. The corresponding logistic model detects size adaptation to a low-energy regime among the smallest primates and, among the primates with the largest brains, thermoregulatory adaptation to the limit on the rate of heat dissipation.

INTRODUCTION

Brain and liver are the two most energy-demanding tissues in mammals, each accounting for ~20% of resting metabolic rate (*rMR*) in humans (6% and 52%, respectively, in mouse) (Elia 1992; Wang et al 2012; Kummitha et al, 2014). The size of the human brain represents a four-fold increase relative to those of other great apes, which in turn are three-fold larger than the brains of gibbons (Smaers et al, 2021; Grabowski et al, 2023; Shao et al, 2023). Since the sizes of the four most thermogenic organs (kidney, heart, liver and brain) scale more or less strictly according body size (Wang et al, 2012), an increase in the absolute size of the brain cannot be accounted for by a decrease in any of the other three organs ("expensive tissue hypothesis" of Aiello and Wheeler, 1995) (Navarette et al, 2011).

Consequently, for a given primate size and resting *MR* (*rMR*), the only way to account for the greater lifetime energy demand of a larger brain is to postulate gains in the reliability of the acquisition and assimilation of food, storage of energy reserves, gestation, lactation and infant care (Mascia-Lees et al, 1986; Koteja, 2000; Fonseca-Azevedo and Herculano-Houzel, 2012; Isler and van Schaik, 2012; Isler and van Schaik, 2014; Kuzawa et al, 2014; Pontzer et al, 2016; Simmen et al, 2017; Grabowski et al, 2023; for review, see Heldstab et al, 2022). However, any account of the change in energy balance associated with a larger brain would not be complete without an explanation of the associated change in thermoregulation: for a given body size and *rMR*, a larger brain implies more rapid internal heat generation accompanied by faster blood perfusion in order to maintain temperature homeostasis (Nybo et al, 2002; Kiyatkin, 2007; Wang et al, 2014). Interestingly, a model of the energy cost of action potential generation predicts a global minimum between 37º - 42ºC (Yu et al, 2012).

A comprehensive biophysical model of thermoregulation in homeothermic mammals envisions a thermogenic core, on the one hand and, on the other, a periphery combining the properties of transport, diffusion, convection and radiation (Porter and Kearney, 2009). This model predicts that for a mammalian *rMR* that scales as $M^{0.75}$, the thermogenic core will scale as $\sim M^{0.50}$ (Porter & Kearney, 2009). We postulated that the combination of four thermogenic organs of mammals serves as a thermoregulatory core ("core model"), estimated organ-specific cellular *MR*s (*cMR*s) consistent with physiological and phylogenetic models, and found that this joint "core" *cMR* scaled as predicted ($M^{0.52}$). We demonstrate that across Euarchontoglires, increases in the relative proportion of the brain *in the core* are offset by decreases in the relative proportion of the liver. Since the liver is the primary organ of gluconeogenesis, this observation is compatible with the energy reliability theory of brain size evolution.

Physiologically-based cMRs do not correspond to log-based sMRs

Assuming a power law model, we distinguish between

specific *MR*s (*sMR*s): $sMR = m \times M^b$,

where *b* is the slope of log *rMR*/log *M*, and

cellular *MR*s (*cMR*s): $cMR = n \times M^c$,

where *c* is the exponent of mass obtained by maximum likelihood fitting to the distribution of a physiologically-relevant trait, such as the number of microRNA families (*mirFam*). Previously, we demonstrated that, unlike *sMR*s, *cMR*s are sensitive to body temperature sample differences in the range of mass (Fromm and Sorger, 2023).

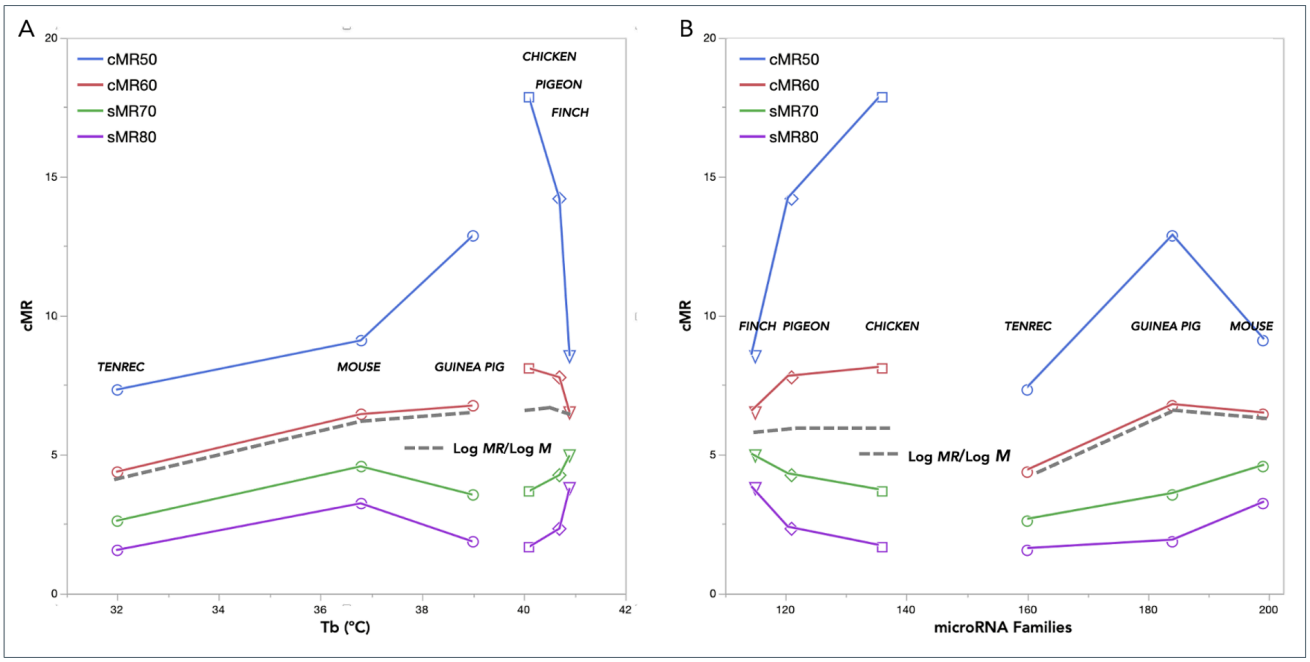

Figure 1. Log-based *sMR*s do not correspond to *mirFam*-based *cMR*s. Data were drawn from Fromm and Sorger (2023). Hatched lines represent the log-based slopes of the birds (*sMR.64*) and the mammals (*sMR.60*). For the purpose of illustration, a difference in T_b of 0.2° C was applied between pigeon and finch. Note the inversion of *cMR* slopes.

Rates of cellular metabolism depend on traits that do not scale logarithmically, such as body temperature (T_b) or the rate of protein synthesis, for which the species-specific number of microRNA families (*mirFam*) may serve as proxy (Fromm and Sorger, 2023). Furthermore, *cMR*s will vary by tissue type and differ between tissues that are renewable or post-mitotic. The rank order of *cMR*s can be matched to non-logarithmic traits by variable allometric scaling, while the rank order of *sMR*s is fixed according to species size (Figure 1).

Cellular *MR*s determine not only the overall slopes of these relationships, but also the order of *cMR*/trait ratios (Figure 2), with implications for models of genetic and phenotypic covariance (Lande, 1979; Felsenstein, 1985; Hansen, 1997; Pagel, 1999; Svensson et al, 2021; Walter and McGuigan, 2023).

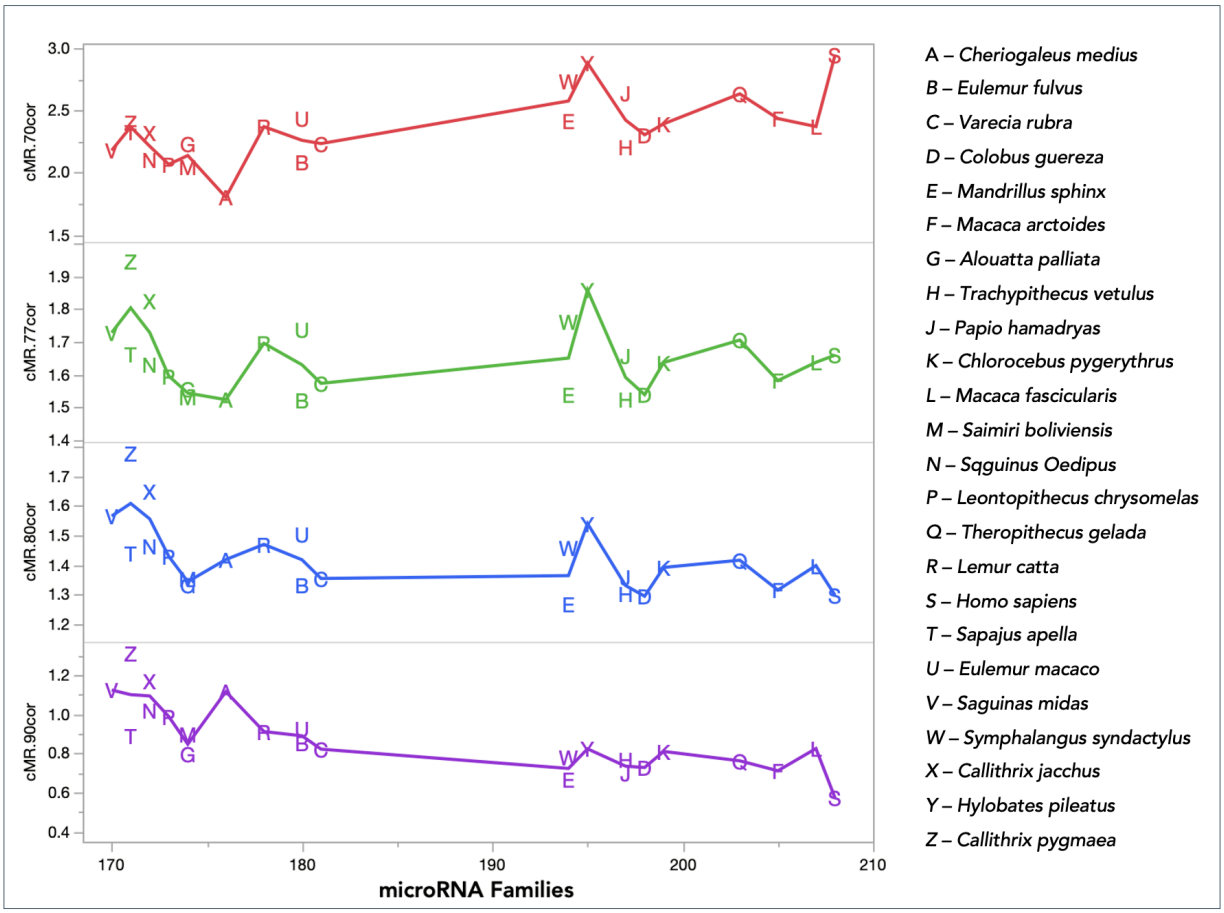

Figure 2. Cellular *MR*s determine the species rank of *cMR*/*mirFam* ratios. Primate species were labeled in order of magnitude of *cMR.75*/*mirFam*, and their distributions plotted as *cMR* was varied. Note the changes in rank order in addition to the changes in overall slope.

In order to develop a thermogenic core model of thermoregulation, we based our estimates of *cMRkdn*, *cMRhrt*, *cMRlvr* and *cMRbrn* in primates on three criteria:

a) size-independent correlation with *mirFam* (physiological relevance);
b) correspondence of the combined *cMR* of these organs with that of the thermogenic core predicted in the biophysical model of Porter & Kearney (2009) (thermodynamic relevance);
c) utility for the unsupervised classification of major primate clades (evolutionary relevance).

We then examined how tradeoffs in the core between brain and liver were related to the divergence of orders and species of Euarchontoglires, and to the corresponding changes in body size and number of microRNA families. Finally, we demonstrate how a logistic model of the relationship between brain size and energy reliability supports the inference of size adaptation to a low energy regime by reduction in size, on the one hand, and thermoregulatory adaptation to the physiological limit on the rate of heat dissipation (hence rate of thermogenesis) in large-brained primates, on the other.

RESULTS AND DISCUSSION

The proportion of brain mass in the core varies reciprocally with that of liver

Of six possible tradeoffs In a core consisting of four thermogenic organs, one major trade off occurs consistently among primate clades, that between brain and liver (Figure 1). A dampened tradeoff between heart and kidney occurs approximately in phase with the major tradeoff.

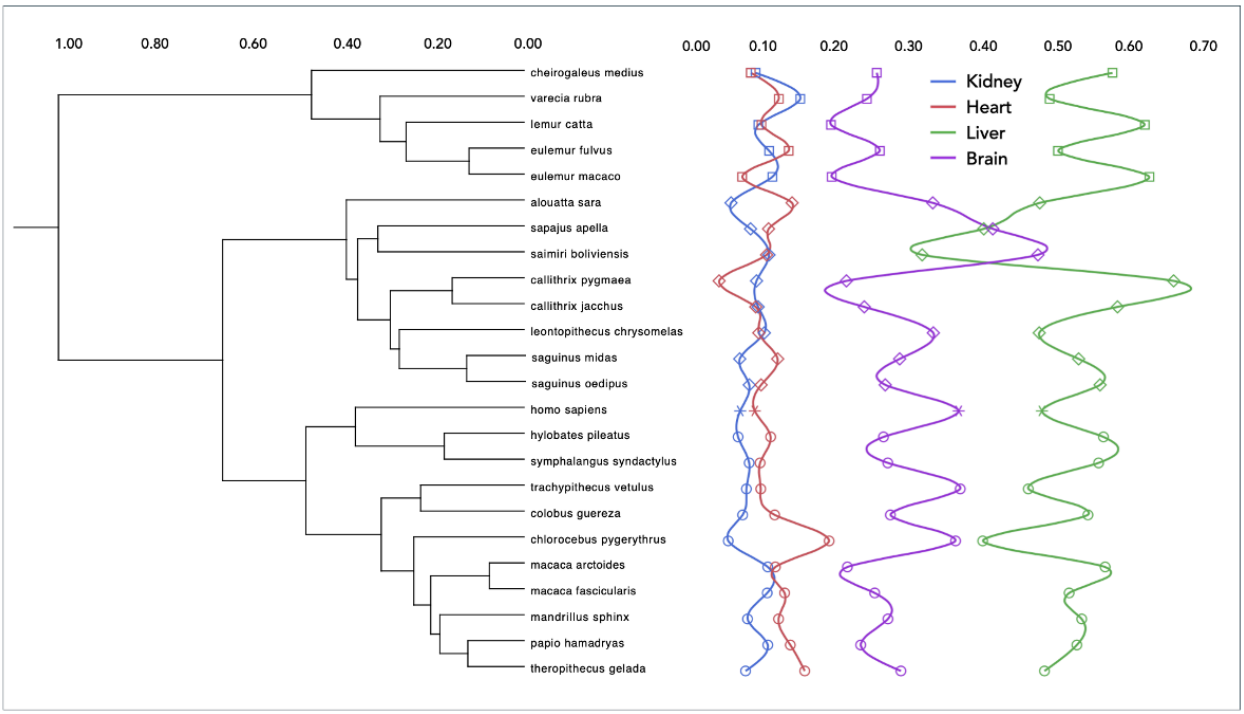

Figure 3. The proportion of brain mass in the core varies reciprocally with that of the liver.

Brain and liver proportions in the core vary reciprocally across 30 additional Euarchontoglires, together with a diminished reciprocity between heart and kidney (Supplementary Figure S1). The observations in primates are summarized geometrically in Figure 4. It is noteworthy that while relative core size (~ $M^{0.50}$) is predicted to decrease with body size (~ $M^{0.75}$) (Porter & Kearney, 2009), the relative core size in humans is greater than that in baboons, which have less than half their body mass.

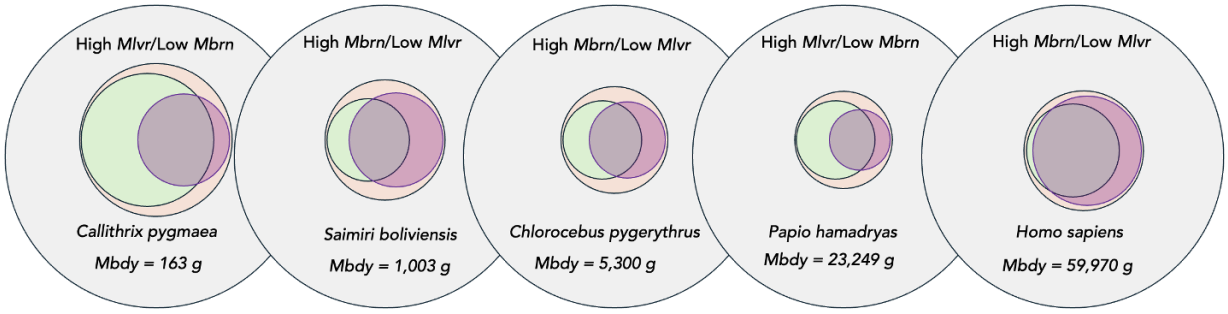

Figure 4. Variation across primates in core size and composition.
The radius of each circle represents a spherical volume corresponding to organ or core mass, scaled to body size (equal circle diameters).

Estimation and physiological relevance of thermogenic organ cMRs

We have previously presented evidence that the number of microRNA families is a statistically and mechanistically credible proxy for the global rate of protein synthesis, which drives 20% of cellular ATP turnover in mammalian cells (Buttgereit and Brand, 1995). We further showed that *mirFam* is an attractor for whole animal *cMR* across the major mammalian clades (Monotreme, Atlantogenata, Laurasiatheria and Euarchontoglires) in a model of stabilizing selection (Fromm and Sorger, 2023). Absent other selective forces, we expected that the diversification of Euarchontoglires would be associated with a steady increase in *cMR* variance with respect to the distribution of *mirFam,* owing to genetic drift and the relaxation of selection.

Figure 5 compares the dependence of *cMR* for each organ on organ size and *mirFam*, together with the log-based *sMR* for each organ. Note the similar trends and inversions among Kidney, Heart and Brain, on the one hand, and Liver and Body, on the other.

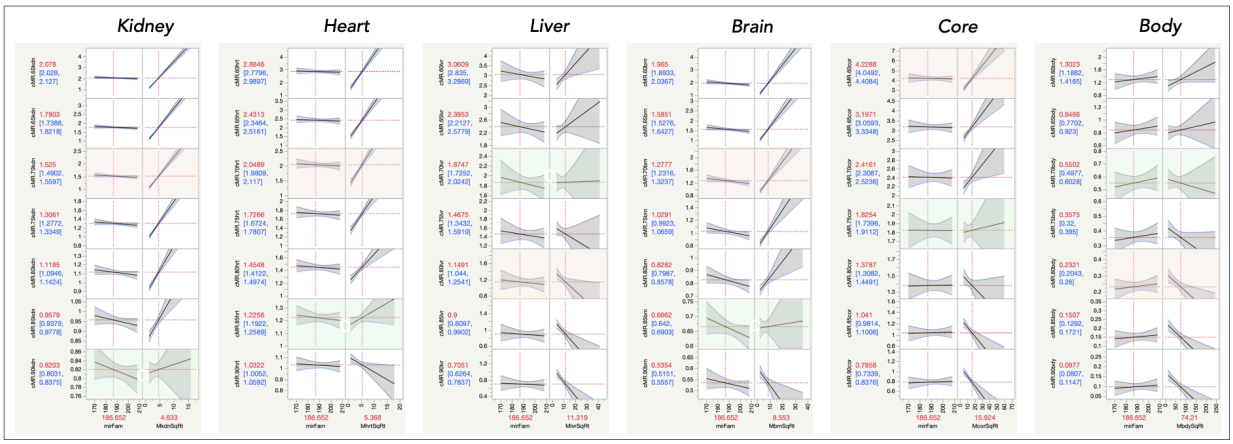

Figure 5. Dependence of *cMR* on √*Morg* and *mirFam* in 23 primates. √*M*, a natural scale for *cMR*s, yields *P* values several orders of magnitude lower than a log scale. Log-based *sMR* slopes are shaded green, *cMR* slopes are shaded pink (see text for detailed explanation).

Figure 6 summarizes these results and compares them to regressions on 27 species of Glires. The Y-axis is an ascending scale of *P* values, which can be interpreted as the degree of release of the constraint of the association with *mirFam*, hence the following order of evolutionary conservation: ***Kdn*, *Hrt* < *Brn* < *Lvr*, *Bdy***. This series comports well with the relative "amplitudes" in the periodic pattern of variation in relative core proportion (Figure 1). Furthermore, the shift to a lower range of *P* values from Glires to Primates is consistent with a shorter time frame for the operation of genetic drift. Comparing the plots for Glires and Primates, there is a leftward shift in the dynamic ranges for liver, and brain cMRs, *i.e.* towards lower allometric exponents, indicating greater dependence on surface area (Figure 6). Given the higher size range among primates, this shift may signal a thermoregulatory adaptation corresponding to a faster rate of heat dissipation. This interpretation is supported by the observation that morphological types, a function of aspect ratios, were significantly related to the number of microRNA families, but not to genome size or the diversity of protein domains (Deline et al, 2018).

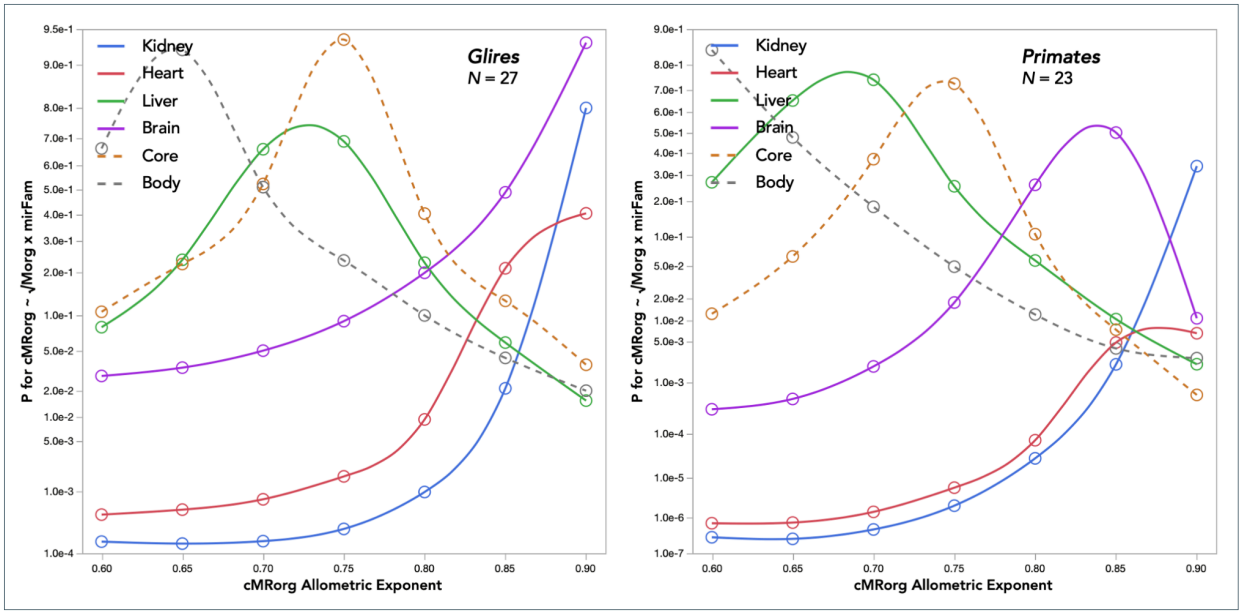

Figure 6. Dependence of *cMR*org on √*Morg* and *mirFam* yields a coherent pattern of variation. Curves were fit by the spline method (*lambda* = 0.00). Note the difference in *P* scales. The primate dataset omitted the largest animal and a small heterotherm (*Homo sapiens* and *Cheirogaleus medius*).

Most striking is the inversion of the relationship with *mirFam* of liver *cMR*s (lower *P* values associated with higher *cMR*s), compared to those of kidney, heart and liver (Figure 4). The *cMRbdy* ~ *Mbdy* correlation tracks that of liver, implying that liver is the organ most affected by thermoregulatory adaptation to changes in animal size. Assuming an operating range of *cMR.70* - *cMR.80* for core and whole body, we estimated the relevant organ *cMR*s as *cMR.70kdn*, *cMR.70hrt*, *cMR.70brn* and *cMR.80lvr*, corresponding to the lowest *P* values in this range, and tested the validity of this combination against thermodynamic and phylogenetic models.

The biophysical model for thermoregulation of Porter & Kearney (2009) envisions a heat-generating "core" and an ellipsoid surround combining the properties of transport, convection, conduction and resistance. For a steady state resting *MR* that scales as $M^{0.75}$, the corresponding rate of core thermogenesis is predicted to scale as ~ $M^{0.50}$ (Porter & Kearney, 2009). As a test of thermodynamic relevance, we compared the predicted allometric scaling of theoretical '*cMR*cor's consisting of the combination of four thermogenic organs, using either log-based *sMR*s or *mirFam*-based *cMR*s:

sMR.Xcor **= (*rMRkdn* + *rMRhrt* + *rMRlvr* + *rMRbrn*) / (*Mkdn* + *Mhrt* + *Mlvr* + *Mbrn*)^{x}**
= (a x *sMR.90*kdn) + (b x *sMR.86*hrt) + (c x *sMR.69*lvr) + (d x *sMR.84*brn)

or

cMR.Xcor **= (a x *cMR.70kdn*) + (b x *cMR.70hrt*) + (c x *cMR.80lvr*) + (d x *cMR.70brn*)**

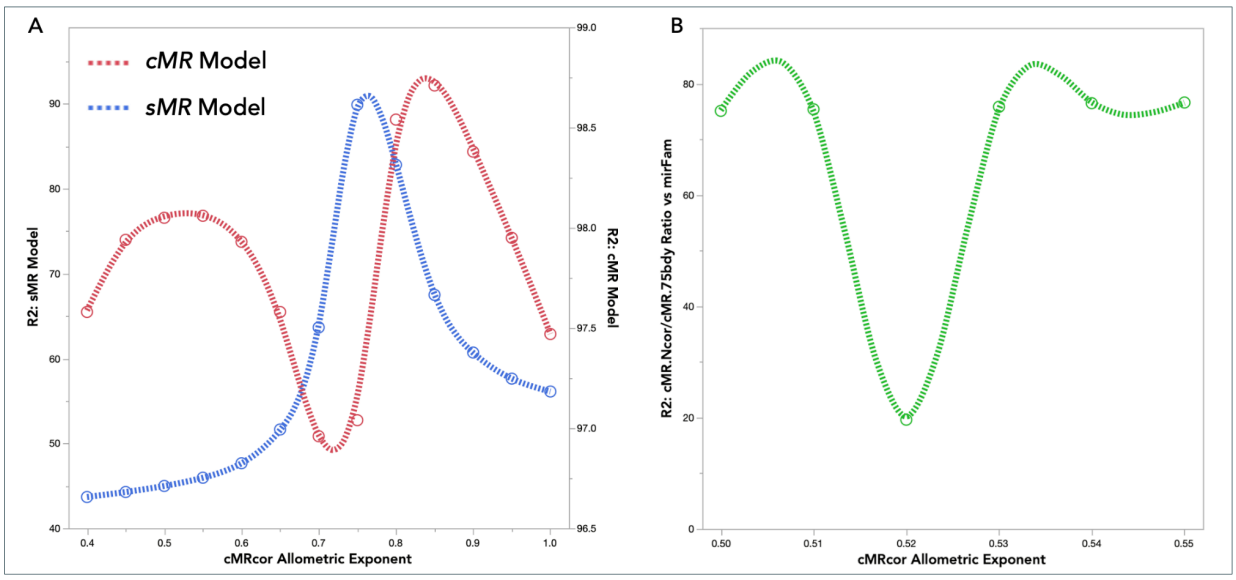

Figure 7. The thermodynamic model of *cMRcor* corresponds to release from *mirFam* constraint.
A. % variation of linear models of *cMR*cor predicted by combinations of log-based *sMR*s or *mirFam*-based *cMR*s of four thermogenic organs for 22 primates (SIMPLS method of partial least squares; deJong, 1993). Note the different scales for the *sMR* and *cMR* models.
B.% variation of dependence of the ratio *cMR.Ncor* *cMR.75bdy* on *mirFam* (51 Euarchontoglires).

The *sMR* model predicted a most probable allometric scaling for this 4-organ core of $M^{0.77}$ (Figure 7), which corresponds to the crossover point for the inversion of slope with respect to mass between *cMR.70* and *cMR.80* (Figures 2 and 5). In contrast, the *cMR* model predicted two possible allometries, one on either side of this inversion (Figure 5), including one that closely matched the predicted allometric scaling of a thermogenic core in the ellipsoid model of thermoregulation (Porter & Kearney, 2009):

*cMR.52*cor = 0.53 x *cMR.70kdn*
+ 0.38 x *cMR.70hrt*
+ 0.36 x *cMR.80lvr*
+ 0.09 x *cMR.70brn*

When regressed against *mirFam*, ratios of *cMR.Ncor/cMR.75bdy* exhibit a sharp minimum at $N = 0.52$, reinforcing our interpretation that the optimal thermodynamic model corresponds to a release from the constraint of the association with *mirFam*.

As a further test of the proposed composition of *cMRcor*, we varied the combinations of organ *cMR*s and found that *mirFam*-based *cMR*s also generated the *cMR*cor corresponding most closely to that predicted by the biophysical model of Porter and Kearney (2009) (Figure 5).

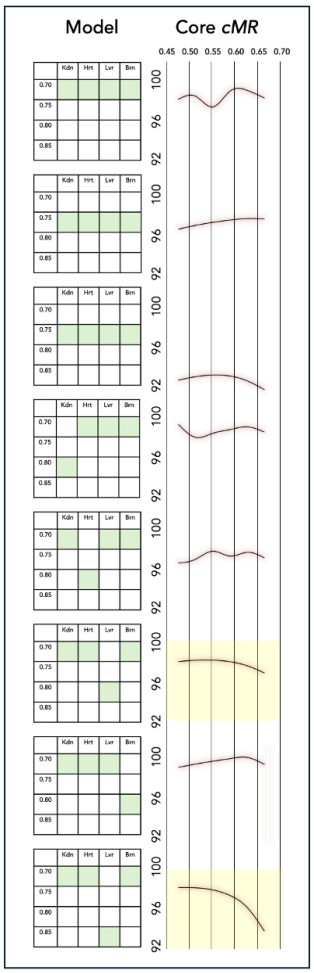

Figure 8. Comparison of core organ *cMR* combinations with respect to the allometric scaling of the corresponding core *cMR*. Each matrix represents one combination of organ *cMR*s, and each trace represents the % variation (R^2) for the predicted *cMRcor* (as in Figure 7).

Two combinations (yellow shading) yielded the lowest optimal core allometric exponent, $M^{0.52}$:

[*cMR.70kdn*, *cMR.70hrt*
***cMR.80lvr*, *cMR.70brn*]**
and
[*cMR.70kdn*, *cMR.70hrt*
***cMR.85lvr*, *cMR.70brn*]**

If our conjecture is correct regarding the relationship between evolutionary constraint and conservation of *cMR* correlations with *mirFam*, then the set of core organ *cMR*s that we have estimated should also be useful in the unsupervised classification of major primate clades. Expectation maximization of Gaussian (normal) mixture models allows the inference of a latent grouping variable, in this case phylogenetic clade. We applied this clustering method to the same 22 primates as in the previous analyses, After varying the *cMR*s for liver, the model with the lowest information criterion was again **[c*MR.70kdn*, *cMR.70hrt*, *cMR.80lvr*, *cMR.70brn*]** (Figure 6).

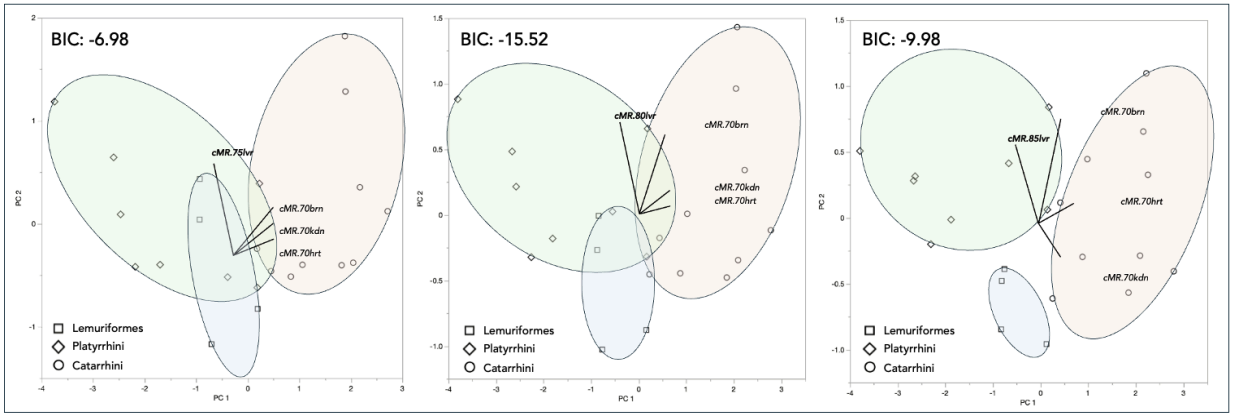

Figure 9. Unsupervised classification of primate clades based on core *cMR* composition. Principal components were calculated from each *cMR* correlation matrix, and membership in two clusters estimated by expectation maximization of their joint probability distributions. Kidney, heat and brain *cMR* = *cMR.70*; liver *cMR*s varied between *cMR.75lvr* - *cMR.85lvr* (bold type). Ellipses were hand-drawn to include all members of the three phylogenetic clades (N = 22).

While *cMR*s were needed to develop and test the core *cMR* concept, tradeoffs between liver and brain *sMR*s are also readily demonstrable with log-transformed data, *provided that they ranked according to core size, not body size*. Figure 10 compares the variation in organ size as a function of body mass (Figure 10A) or core mass (Figure 10C). Examination of the residuals of the corresponding regressions reveals a periodic pattern of variation for each organ, corresponding to their relative proportion of body mass (Figure 10B) or core mass (Figure 10D). The periodicity is a function of autocorrelation, as can be easily demonstrated when the analysis is limited to a single pair of organs (Figure 11). A consistent tradeoff between brain and liver extending across the entire range is apparent only when organ masses are standardized against core mass (Figure 10D versus Figure 10B). In other words, standardization of log *Mbrn* against log *Mbdy* precludes detection of this tradeoff (Navarette al, 2011).

Tradeoffs in the evolution of organ cMRs conform to the core model of thermoregulation.
The evolutionary histories of the four organ *cMR*s provides compelling evidence that they have been constrained by their relationship to the core. We examined how the tradeoffs between brain and liver were related to the divergence of orders and species of Euarchontoglires, and to the corresponding changes in body size and number of microRNA families (Figure 12).

While the *cMR.80lvr* tree mirrored that of body size, the tree for *cMR.70brn* largely resembled that of *mirFam* (Figure 12), exhibiting a sharp contrast between the relative arrest in the rate of evolution of *cMR.70brn* upon the divergence of Glires, and acceleration leading up to the divergence of Catarrhini. Furthermore, relative to the Haplorrhini, the evolution of *cMR.70brn* was relatively arrested in the Lemuriform (Strepsirrhini) clade (Figure 12). The inference of an exceptional rate of brain size increase in humans attests to the validity of the variable rate model's default expectation of a Brownian process of genetic drift (Pagel et al, 2004).

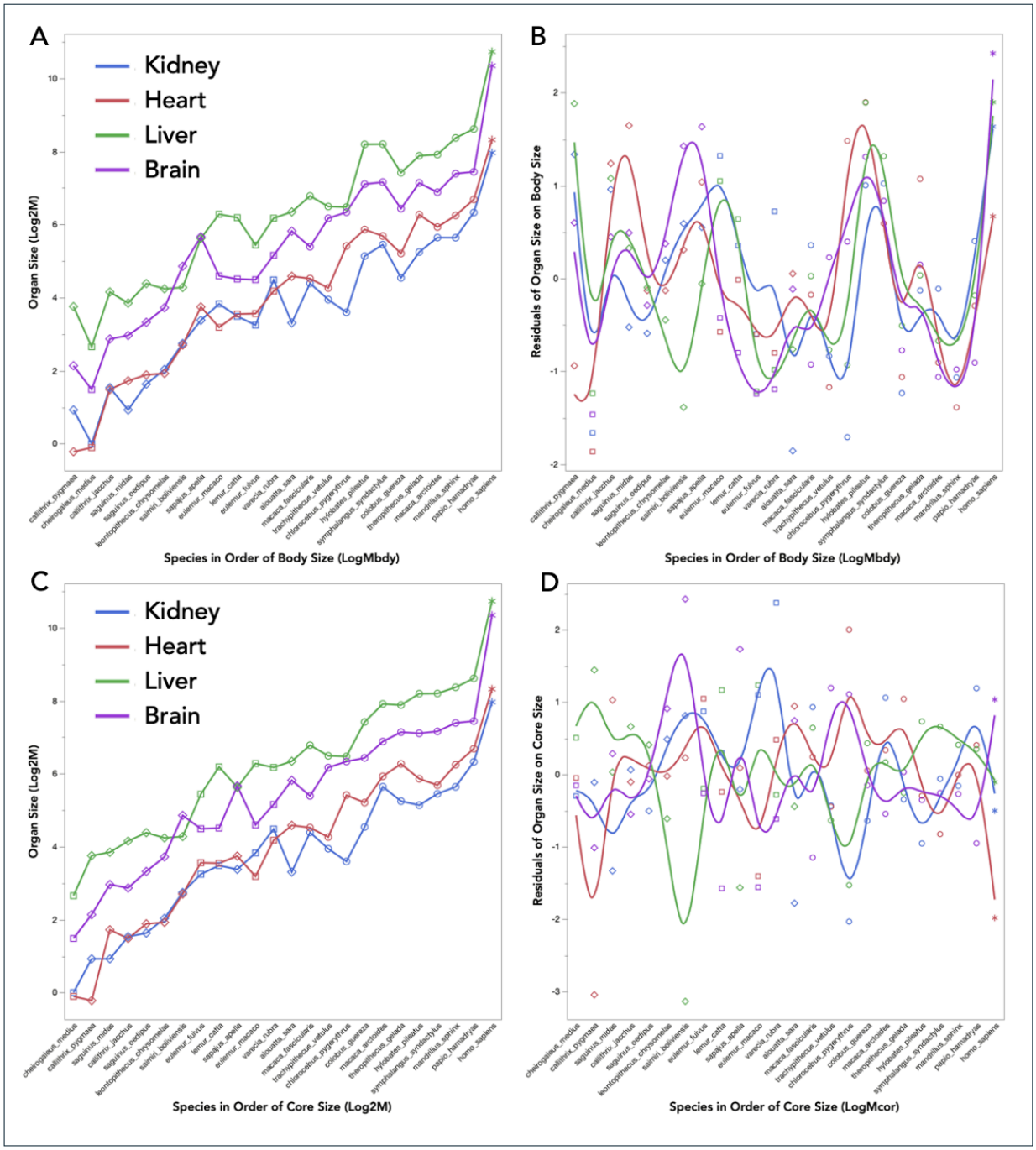

Figure 10. Reciprocal variation between liver and brain is a function of core size.
A and C: Variation of organ size relative to body size and core size in primates.
B and D: Residual variation relative to body size and core size in primates.

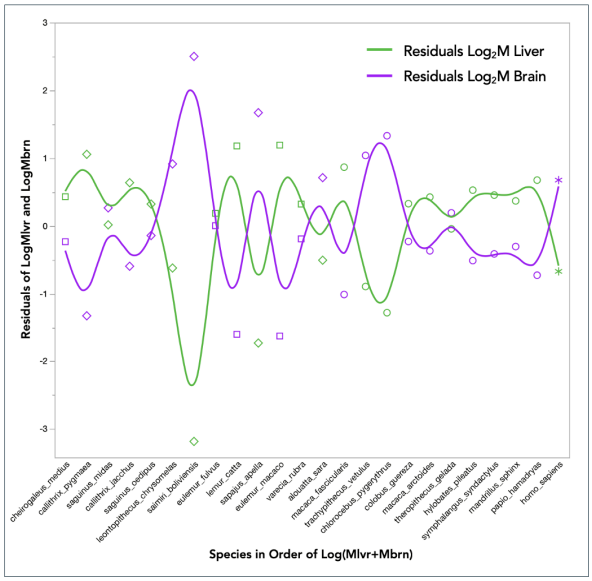

Figure 11. Tradeoffs between liver and brain as a function of their combined mass. The “phase shift” between the residuals of liver and brain with respect to the core (Figure 7D) can be isolated by repeating the regression with respect to Log (*Mlvr* + *Mbrn*), demonstrating that the periodicity depends on autocorrelation.

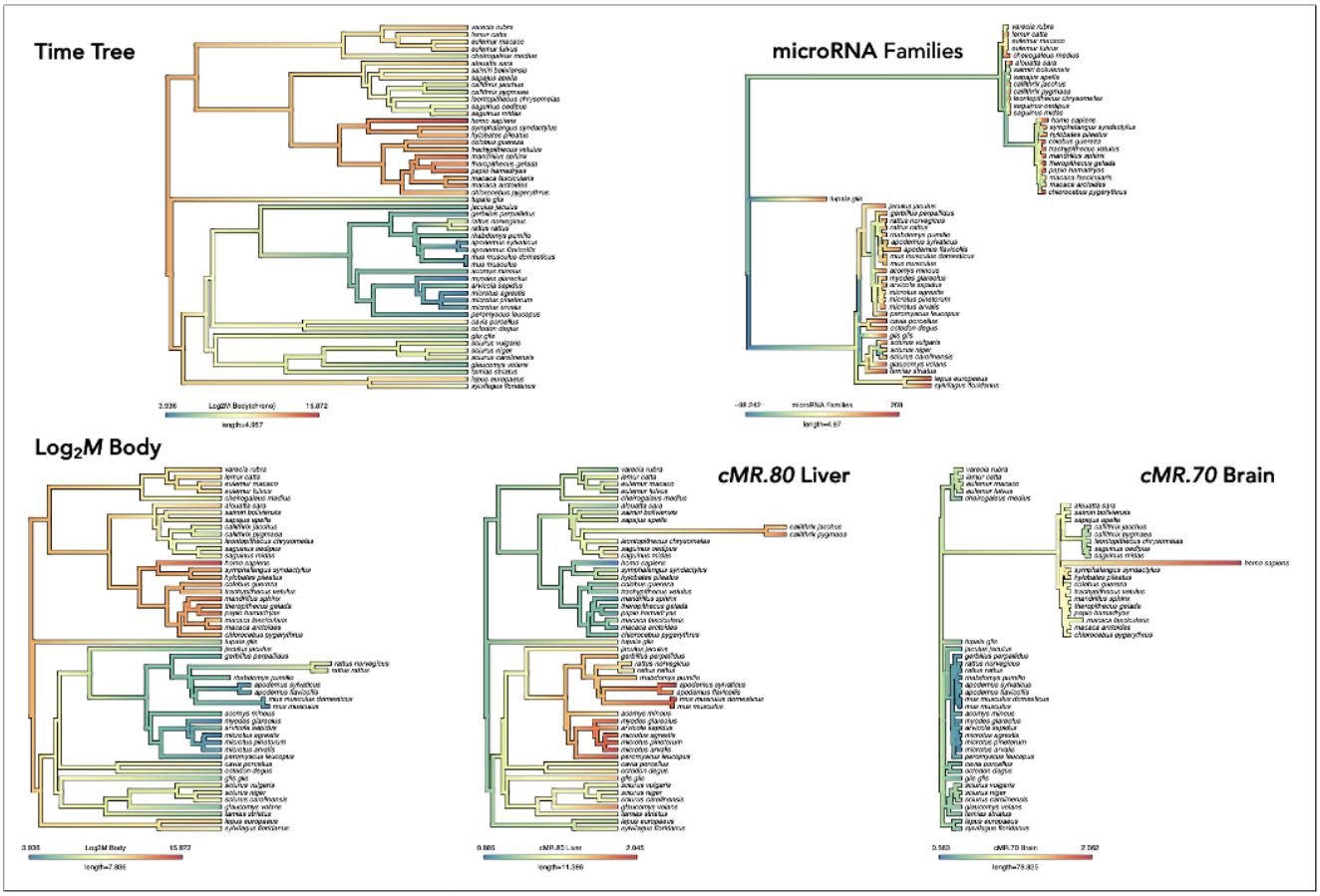

Figure 12. Time tree and variable rate phenograms of Log_2*Mbdy*, *mirFam*, *cMR.80lvr* and *cMR.70brn*. The node values for Log_2*Mbdy* were also applied to the time tree, in order to contrast the branch lengths. Bayes Factors for the variable rate trees ranged from 15.18 (Log_2*M*) to 37.94 (*mirFam*).

The two smallest Platyrrhini, one of which (*Callithrix pygmaea*) is a suspected heterotherm (Tattersall, 2012), exhibited exceptional increases in *cMR.80lvr*, consistent with adaptation to a low energy regime

and increased reliance on gluconeogenesis. However, the most striking contrasts are the opposing *cMRlvr* - *cMRbrn* tradeoffs between Primates and Glires (Figure 12).

Heart *cMR.70* generally tracked the difference between Glires and primates in body size evolution, with a contrast in evolutionary rates between an acceleration among Catarrhini and the two largest Glires (Lagomorphs), on the one hand, and the relative arrest among the smaller Glires, on the other (Figure 13). Relative kidney *cMR.70* levels generally corresponded to those of heart, while the relative rates of evolution were generally diminished except for the accelerated rate for human *cMR.70kdn*, suggesting adaptation to an altered landscape of opportunities for hydration *versus* risks of dehydration.

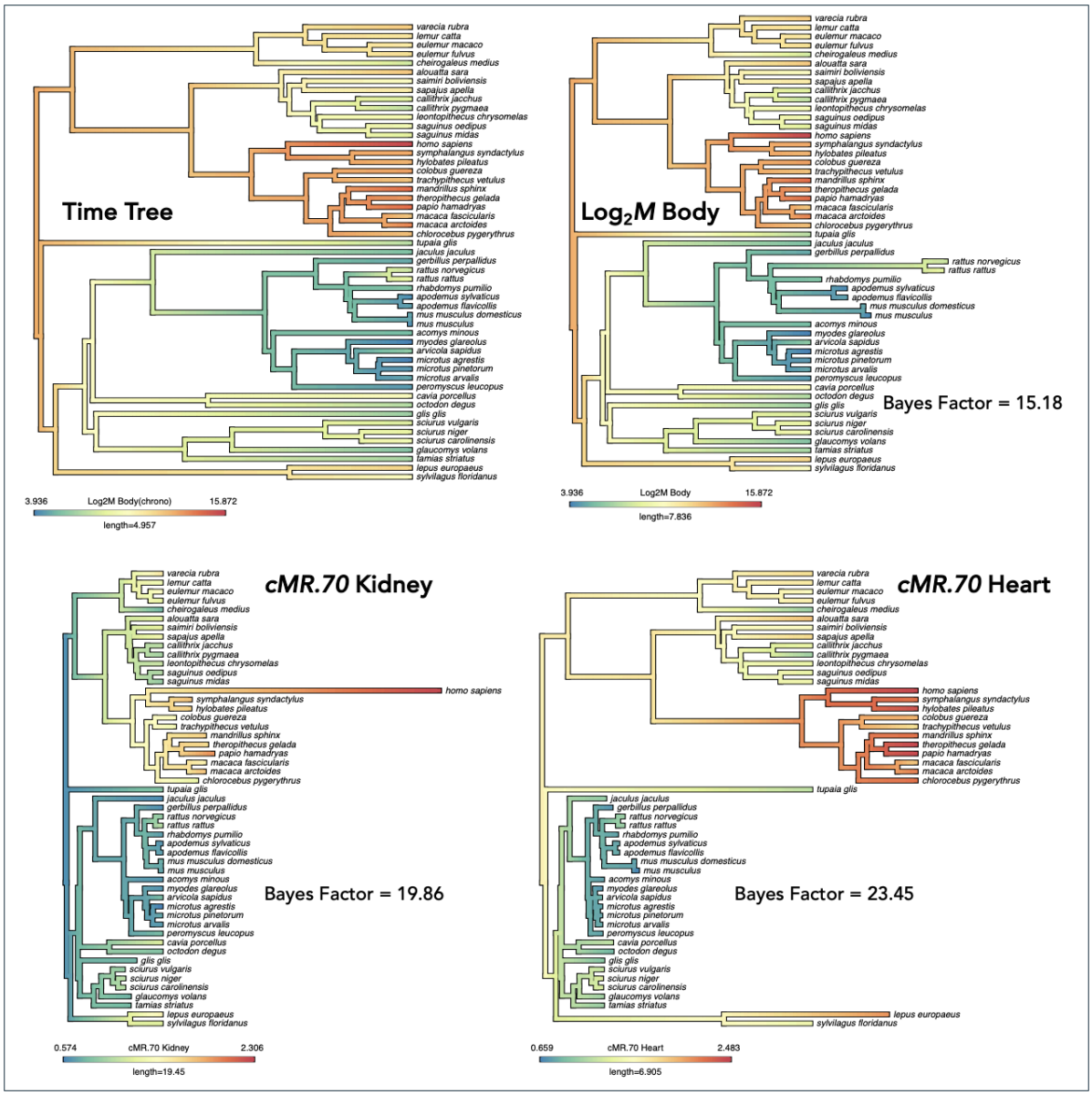

Figure 13. Variable rate phenograms comparing the evolution of kidney and heart *cMR*s to the evolution of body size.

SUMMARY AND CONCLUSIONS

Linearization of distributions of body mass and metabolic rate by log transformation has been *de rigueur* for phylogenetic comparative studies. Unlike log-derived *sMR*s, the c*MR*s of core thermogenic organs can be estimated according to physiological, thermodynamic and phylogenetic criteria. They can also be linearized with respect to the corresponding rate of thermogenesis of a four-organ core (Figure 14). Only the latter method reveals the inverse relationship between brain and liver *cMR*s.

Countless comparative studies of whole body *rMR* in mammals have yielded *sMR* exponents ~ 0.75. Our analysis reveals that *cMR.75* corresponds approximately to the midpoints of the dynamic ranges of the *mirFam* correlations with *cMRlvr* ~ √*Mlvr* and *cMRbrn* ~ √*Mbrn* (Figure 6). Importantly, the interval between *cMR.*70 - *cMR.80* represents the region of minimal *mirFam* constraint on the core *cMR* (*cMR.75cor*). In other words, "Kleiber's Law" for the log-based allometric scaling of mammalian *rMR* (Kleiber, 1934; Balllesteros et al, 2018) corresponds to the zone of weakest association between the core rate of thermogenesis and the global microRNA *milieu*.

The recent addition of hundreds of primate genome sequences (Kuderna et al, 2024) has been accompanied by ever more fine-grained studies of the covariance of traits suspected to influence the evolution of brain size. For the reasons elaborated in the Introduction, we submit that a fundamental assumption underlying these analyses – that brain energy expenditure varies with log-transformed brain mass or volume in a manner consistent with thermoregulatory constraints – is not justified.

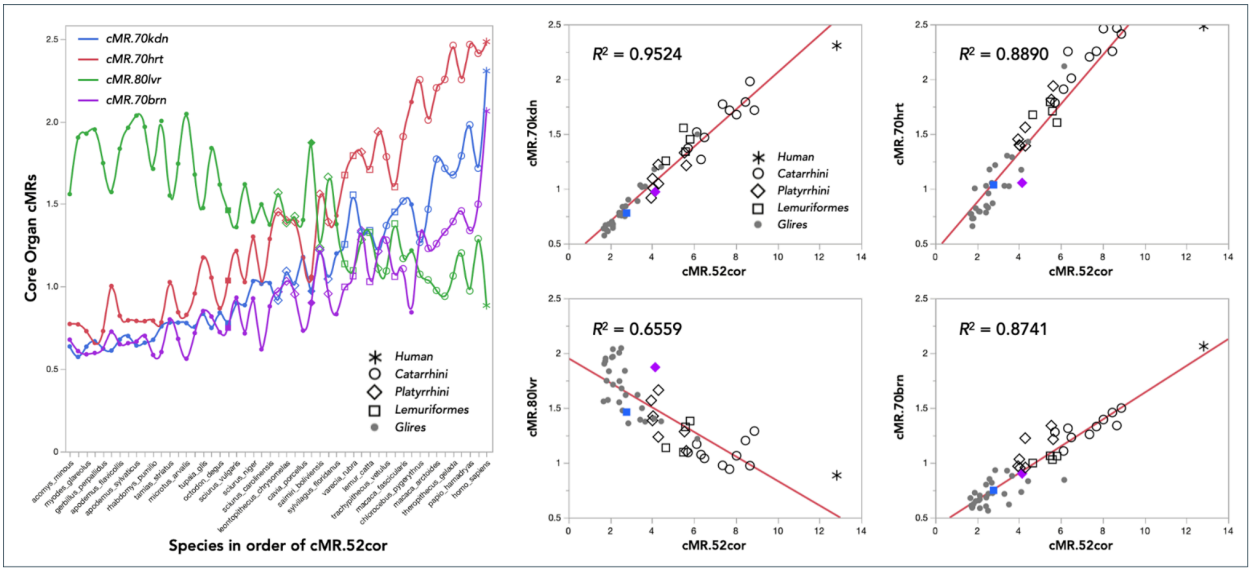

Figure 14. The thermodynamic origin of tradeoffs among core organ *cMR*s.
A. Species organ *cMR*s are proportional to the predicted species rate of core thermogenesis.
B. Linear regressions of individual organ *cMR*s on the *cMR* of the model thermogenic core.

Of the six possible tradeoffs in *cMR* among the four thermogenic organs, why is the brain-liver tradeoff the most significant? In a prolonged state of fasting, the liver is the primary organ of gluconeogenesis:

the glucagon-dependent reduction of amino acid backbones fueled by free fatty acids released from adipose tissue. If an evolutionary increase in reliability of the energy supply meant a decrease in the frequency of prolonged fasting, hence reliance on gluconeogenesis, retaining the ancestral liver size and *cMR* would have been inefficient. This dynamic would have been reinforced if brain enlargement meant greater reliability of the energy supply.

We propose the following example of a *cMR*-based model of brain size evolution based on a simple feedback loop between brain size and the reliability of the energy supply: improvements in energy reliability facilitate increases in brain size, which in turn favor further improvements in energy reliability, up to the limits imposed by anatomy and physiology *e.g.* the diameter of the birth canal and the physiological limit on the rate of heat dissipation (Speakman and Król, 2010). This neutral model reduces several current hypotheses (Expensive Brain/Ecological Brain/Cognitive Buffer) (Heldstab et al. 2022) to one that does not presuppose any underlying mechanism. It is a classic logistic model, with cMR_{max} standing in for carrying capacity in a population logistic model:

$$\mathbf{d(}\boldsymbol{cMRbdy}\mathbf{)\ /\ d(}\boldsymbol{Vbrn}\mathbf{)\ =\ }\boldsymbol{r}\mathbf{\ \bullet\ }\boldsymbol{cMRbdy}\mathbf{\ [1\ -\ (}\boldsymbol{cMRbdy}\mathbf{\ /\ }\boldsymbol{cMR}_{\mathbf{max}}\mathbf{)]}$$

where *r* is a rate constant and the range of *cMRbdy* has been standardized to 1.00.

We applied this model to the primate brain size dataset of Grabowski et al (2023), fitting it to *mirFam*, a proxy for *cMRbdy i.e.* the overall rate of energy utilization (Figure 15A). Unexpectedly, the model revealed that relative brain size is a predictor of *mirFam*, rather than *vice versa*, lending credence to the proposition that larger brains were associated with improvements in the reliability of the energy supply.

Given that the relative sizes of the three other thermogenic organs also fit logistic models for *mirFam* (Supplementary Figure S2), the question arises as to which relationship is the principal driver of adaptation. In phylogenetic regressions for organ *cMR*s ranging from *cMR*.60 - *cMR*.80, kidney, heart and liver *cMR*s varied independently of phylogeny (Pagel's *lambda* = 0), while the variation of brain *cMR*.60 - *cMR*.80 with respect to *mirFam* was secondary to phylogenetic distance (Pagel's *lambda* = 1 in each case), suggesting that the divergence of primate species largely coincided with changes in the relationship of *mirFam* to brain mass and *cMR* (Supplementary Table S3) (Pagel, 1999).

Returning to the logistic model based on relative brain size, a variable rate phenogram for primate species was generated using the ratios from a Hubbert linearization of the logistic function (Figure 15B) (Hubbert, 1982). Thus, the color scale represents the rank on the logistic curve which, in general, tracks body size (compare with the Log_2M panel in Figures 12 and13). The three smallest species, a Lemuriform and a pair of Callitrichinae, exhibited an accelerated rate of descent in rank. *Cheirogaleus medius* is a heterotherm, and *Callithrix pygmaea* may also be heterothermic (Tattersall, 2012),

indicating that the baseline of the logistic function represents a regime of minimal energy reliability, perhaps related to low calorie-density folivory or insectivory.

Following this logic, we can ask what sort of constraint might be encountered near the plateau of this model? A likely candidate would be the physiological limit on the rate of heat dissipation (Speakman and Król, 2010; Fromm and Sorger, 2023). During exercise with progressive hyperthermia, human brain temperature increases in parallel with that of the body core, leading to hyperthermia and fatigue (Nybo, 2012; Nybo and González-Alonso, 2015; Tsuji et al, 2016). Over a period spanning 700,000 years of human evolution, body mass and shape varied inversely with temperature, indicative of selection in response to thermoregulatory demands (Stibel, 2023).

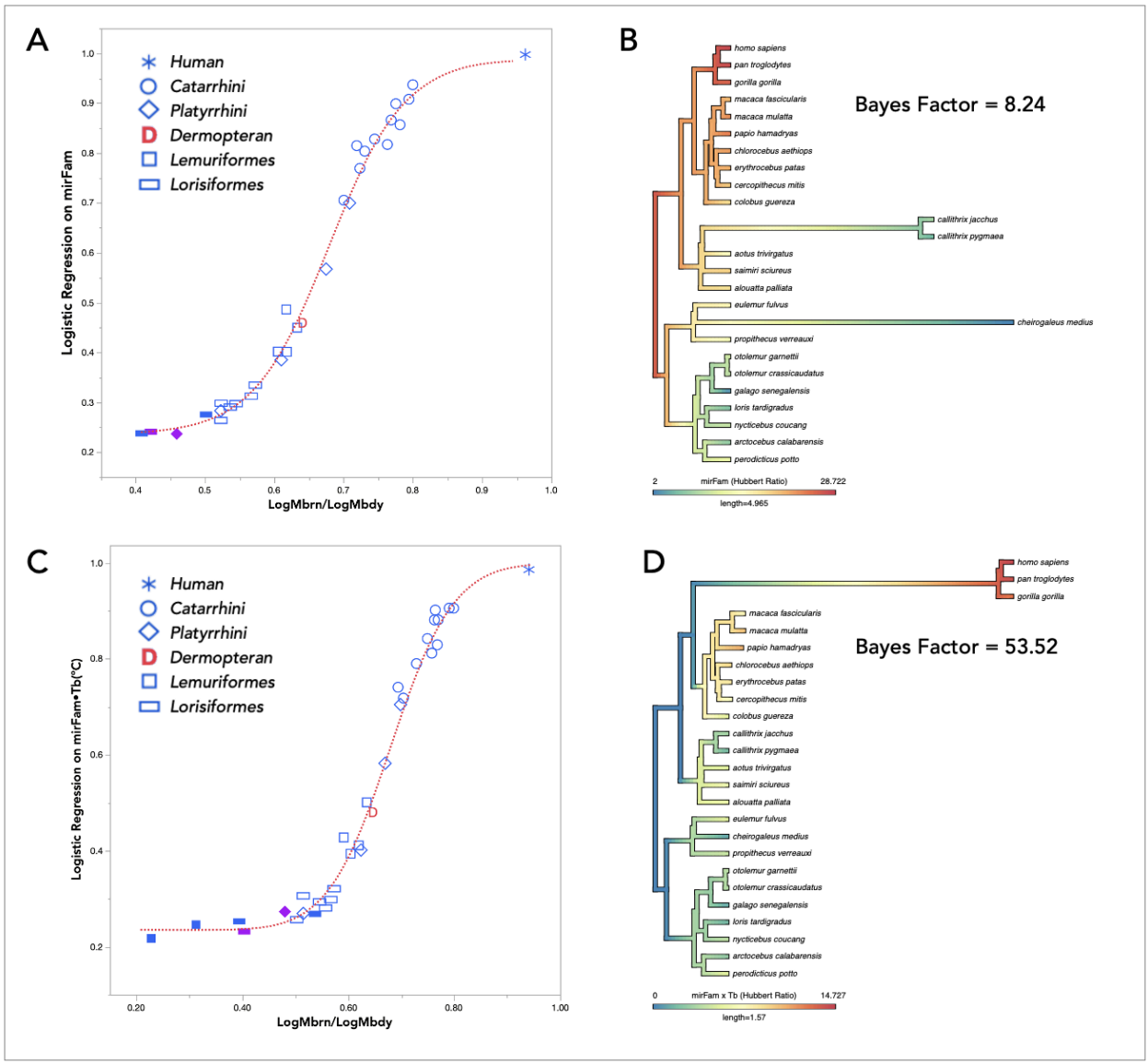

Figure 15. Logistic models of brain size evolution (data from Grabowski et al, 2023).
A, C. For these idealized models (R^2 = 1.00), *mirFam* or *mirFam•*T_b(ºC) was that predicted by the original logistic regression model (R^2 = 0.90 and 0.86, respectively) (jitter applied).
Filled symbols: heterotherms (blue), suspected heterotherms (purple). D = *Galeopterus variegatus*.
B, D. Variable rate phenograms of the Hubbert linearization of the logistic functions.

Previously we reported several observations indicating a reciprocal relationship in the evolution of body temperature and metabolic rate: in the case of primates, body temperatures (T_b) were inversely correlated with *mirFam* (Fromm and Sorger, 2023). This conserved nature of this relationship can be visualized by ranking primate species according to the product of T_b x *mirFam* (Supplementary Figure S3). We hypothesized that this product is representative of the heat dissipation limit; in this case, accelerated evolution near the plateau of a T_b x *mirFam* logistic model might signal a thermoregulatory adaptation. This indeed appears to be have been the case for the divergence of hominid apes (Figure 15C, D) and accords well with the disproportionate increase in the mass of the 4-organ thermogenic core that accompanied the enlargement of the primate brain (Figure 4) and the leftward shift in the *mirFam* correlation profiles for brain and liver (Figure 6). If our interpretation of these models is correct, then the Bayesian inference of opposite evolutionary trends depicted on the phenograms, descending in rank on the *mirFam* tree, and ascending in rank on the tree for *mirFam* x T_b, would assign the ancestral primate a high rank with respect to energy reliability and a low rank with respect to the heat dissipation limit, a propitious combination for the founder of a new order of mammals.

METHODS

Physiological Data

The masses and *rMR*s of the four thermogenic organs were obtained from the dataset of Wang et al (2012), itself mainly derived from the compilation of Navarette et al (2011) (Supplementary Table S1).

MicroRNA Families

Complements of microRNA families were obtained from the most complete assembly for each species using covariance model MirMachine (Umu et al, 2023), trained on the manually-curated database MirGeneDB2.1 (Fromm et al 2021).

Phylogenetic Trees

Using Mesquite © (2021) we derived ultrametric trees for 51 Euarchontoglires or 25 primates from the phylogenies of Alvarez-Carretero et al (2021) and Shao et al (2023), respectively.

Variable Rate Phenograms

Variable rate trees and ancestral node values were inferred using BayesTraits.V4 (Pagel, 1999; Pagel et al, 2004; Venditti et al, 2011) (software available at www.evolution.rdg.ac.uk). Bayes factors for variable rate trees were computed from the difference between the median of the top 1% likelihoods and the median likelihood of the trees with lowest 1% sum of changes to branch length (Fromm and Sorger, 2023). Phenograms were generated using Phytools (Revell, 2012).

Statistics

Linear, partial least squares, and logistic regressions and normal mixture clustering were carried out and visualized using JMP16 ®. All R^2 values were adjusted for the number of predictors. Phylogenetic linear regressions were carried out using the R: CAPER package (Orme, 2013).

DATA AVAILABILITY

The original data with accompanying references and the results of all analyses referred to in the text are provided in the Supplementary Information (below).

ACKNOWLEDGMENT

BF is supported by the Tromsø forskningsstiftelse (TFS) [20_SG_BF 'MIRevolution'].

AUTHOR CONTRIBUTIONS

Conceptualization: TS; Methodology: TS; Investigation: BF and TS; Writing – Original Draft: TS; Writing – Review & Editing: BF and TS; Visualization: BF and TS; Funding Acquisition: BF.

DECLARATION OF INTERESTS The authors declare no competing interests.

REFERENCES

Aiello LC and Wheeler P. 1995. The expensive-tissue hypothesis: the brain and the digestive system in human and primate evolution. *Curr Anthro* 36: 199-221.

Álvarez-Carretero S, Tamuri A, Battini M, Nascimento F, Carlisle E, Asher R, Yang Z, Donoghue P and Dos Reis M. 2022. A species-level timeline of mammal evolution integrating phylogenomic data. Nature 602: 263-267.

Ballesteros FJ, Martinez VJ, Luque B, Lacasa L, Valor E and Moya A. 2018. On the thermodynamic origin of metabolic scaling. *Scientific Reports* 8: 1448.

Buttgereit F and Brand MD. 1995. A hierarchy of ATP-consuming processes in mammalian cells. Biochem J 312: 163-167.

de Jong (1993). SIMPLS: An alternative approach to partial least squares regression. *Chemometrics and Intelligent Laboratory Systems*, 18: 251–263.

Deline B, Greenwood JM, Clark JW, Puttick MN, Peterson KJ, Donoghue PCJ. 2018. Evolution of metazoan morphological disparity. *PNAS* 29: E8909-E8918.

Elia M. Organ and tissue contribution to metabolic rate. 1992. In: Kinney JM, Tucker HN (eds), Energy metabolism: tissue determinants and cellular corollaries. pp 61-80. (Raven Press, NY).
Pagel M. 1999. Inferring the historical patterns of biological evolution. *Nature* 401: 877-884.
Felsenstein J. 1985. Phylogenies and the comparative method. *Amer Naturalist* 125: 1-15.

Fonseca-Azevedo K and Herculano-Houzel S. 2012. Metabolic constraint imposes a tradeoff between body size and number of brain neurons in human evolution. *PNAS* 109: 18571-18576.

Fromm B, Høye E, Domanska D, Zhong X, Aparicio-Puerta E, Ovchinnikov V, Umu SU, Chabot, PJ, Kang W, Aslanzadeh M, Tarbier M, Mármol-Sánchez E, Urgese G, Johansen M, Hovig E, Hackenberg M, Friedländer MR and Peterson KJ. 2021. MirGeneDB 2.1: toward a complete sampling of all major animal phyla. *Nucl Acids Res* 50: D204-D210.

Fromm B and Sorger T. 2023. Rapid adaptation of cellular metabolic rate to the microRNA complements of mammals and its relevance to the evolution of endothermy. *iScience*: 108740.

Grabowski M, Kopperud BT, Tsuboi M and Hansen TF. Both diet and sociality affect primate brain-size evolution. *Syst Biol* 72: 404-418.

Hansen TF. 1997. Stabilizing selection and the comparative analysis of adaptation. *Evolution* 51: 1341-1351.

Heldstab SA, Isler K, Graber SM, Schuppli C and van Schaik. The economics of brain size evolution in vertebrates. *Curr Biol* 32: R697–R708.

Hubbert MK. 1982. Techniques of prediction as applied to the production of oil and gas. In Gass, Saul I. (ed.). Oil and Gas Supply Modeling (proceedings of a symposium held at the Department of Commerce, Washington, DC, June 18–20, 1980). NBS Special Publication 631. Washington (DC): National Bureau of Standards. pp. 16–141.

Isler K and van Schaik CP. 2012. Allomaternal care, life history and brain size evolution in mammals. *J Human Evol* 63: 52 - 63.

Isler K and van Schaik CP. 2014. How humans evolved large brains: comparative evidence. *Evol Anthropol* 23: 65-75.

Kiyatkin AE. 2007. Brain temperature fluctuations during physiological and pathological conditions. *Eur J Appl Physiol* 101:3-17.

Kleiber M. 1932. Body size and metabolism. *Hilgardia* 6: 315-353.

Koteja P. 2000. Energy assimilation, parental care and the evolution of endothermy. *Proc Roy Soc B* 267: 479-484.

Kuderna LFK, Gao H, Janiak MC . . . Bonet TM. 2023. A global catalog of whole-genome diversity from 233 primate species. *Science* 380: 9-60913.

Kummitha CM, Kalhan SC, Saidel GM and Lai N. 2014. Relating tissue/organ energy expenditure to metabolic fluxes in mouse and human: experimental data integrated with mathematical modeling. *Physiol Rep* e12159 (1-20).

Kuzawa CW, Chugani HT, Grossman LI, Lipovich L, Muzik O, Hof PR, Wildman DE, Sherwood CC, Leonard WR and Lange N. 2014. *PNAS* 111: 13010-13015.

Lande R. 1979. Quantitative genetic analysis of multivariate evolution, applied to the brain: body size allometry. *Evolution* 33: 402-416.

Magalhães JP, Abidi Z, dos Santos GA . . . Ka Po To P. 2024. Human Ageing Genomic Resources: updates on key databases in ageing research. *Nucl Acids Res* 52: D900-D908.

Mascia-Lees FE, Relethford JH and Sorger T. 1986. Perspectives on permanent breast enlargement in human females. *Amer Anthro* 88: 423-428.

Nybo L. 2012. Brain temperature and exercise performance. *Exp Physiol* 97: 333-339.

Nybo L, Secher NH and Nielsen B. 2002. Inadequate heat release from the human brain during prolonged exercise with hyperthermia. *J Physiol* 545: 697-704.

Nybo L and González-Alonso J. 2015. Critical core temperature: a hypothesis too simplistic to explain hyperthermia-induced fatigue. *Scand J Med Sci Sports* 25: 4-5.

Navarette A, van Schaik CP and Isler K. 2011. Energetics and the evolution of human brain size. *Nature* 480: 91-93.

Orme D, Freckleton RP, Thomas GH and Petzoldt T. 2013. CAPER: comparative analyses of phylogenetics and evolution in R. *Methods Ecol and Evol* 3: 141-151.

Pagel M. 1999. Inferring the historical patterns of biological evolution. *Nature* 401: 877-884.

Pagel M, Meade A and Barker D. 2004. Bayesian estimation of ancestral character states on phylogenies. *Syst Biol* 53: 673-684.

Pontzer H, Brown MH, Raichlen DA . . . Ross SR. 2016. Metabolic acceleration and the evolution of human brain size and life history. Nature 533: 390-393.

Porter WP and Kearney M. 2009. Size, shape, and thermal niche of endotherms. *PNAS* 106: 19666-19672.

Revell LJ. 2012. phytools: an R package for phylogenetic comparative biology (and other things). *Methods Ecol Evol* 3: 217–223.

Shao Y, Zhou, Li F . . . Wu DD. 2023. Phylogenomic analyses provide insights into primate evolution. *Science* 380: 913-924.

Simmen B, Pasquet P, Masi S, Koppert GJA, Wells JCK and Hladik CM. 2017. Primate energy input and the evolutionary transition to energy-dense diets in humans. *Proc Roy Soc B* 284: 20170577.

Smaers JB, Rothman RS, Hudson DR, Balanoff AM, Beatty B, Dechmann DKN, deVries D, Dunn, JC, Fleagle JG, Gilbert CC, Goswami A, Iwaniuk AN, Jungers WL, Kerney M, Ksepka DT, Manger PR, Mongle CS, Rohlf FJ, Smith NA, Soligo C, Weisbecker V and Safi K. 2021.
The evolution of mammalian brain size. *Sci Adv* 7: eabe2101 (1-11).

Speakman JR and Król E. 2010. Maximal heat dissipation capacity and hyperthermia risk: neglected key factors in the ecology of endotherms. J Anim Ecol 79: 726–746.

Stibel JM. 2023. Climate change credictive of body size and proportionality in humans. *Evol Biol* 50: 461-475.

Svensson EI, Arnold SJ, Bürger R et al. 2021. Correlational selection in the age of genomics. *Nat Ecol Evol* 5, 562–573.

Tattersall GJ. 2012. Diurnal changes in metabolic rate in pygmy marmosets: Implications for sleep, torpor, and basal metabolism in primates. In: Ruf, T., Bieber, C., Arnold, W., Millesi, E. (eds) Living in a Seasonal World, chapter 41: 471-480. Springer.

Tsuji B, Hayashi K, Kondo N and Nishiyasu T. 2016. Characteristics of hyperthermia-induced hyperventilation in humans. *Temperature* 3: 146–160.

Umu SU, Paynter VM, Trondsøn H, Buschmann T, Rounge TB, Peterson KJ and Fromm B. 2023. Accurate microRNA annotation of animal genomes using trained covariance models of curated microRNA complements in MirMachine. *Cell Genomics* 3, 100348.

Venditti C, Meade A. and Pagel M. 2011. Multiple routes to mammalian diversity. *Nature*, 479, 393-396.

Walter GM and McCuigan K. 2023. Phenotypic evolution: predicting the future. *eLife* 12: e91450 (1-3).

Wang H, Wang B, Normoyle K, Jackson K, Spitler K, Sharrock MF, Miller CM, Best C, Llano D and Du R. 2014. Brain temperature and its fundamental properties: a review for clinical neuroscientists. *Front Neurosci* 307: 1-17.

Wang ZM, Zhang J, Ying Z and Heymsfield SB. 2012. Organ-tissue level model of resting energy expenditure across mammals: new insights into Kleiber's Law. *ISRN Zool*: 673050 (1-9).

Yu Y, Hill AP and McCormick DA. 2012. Warm Body Temperature Facilitates Energy Efficient Cortical Action Potentials. *PLoS Comp Biol* e1002456: 1-16.

SUPPLEMENTARY INFORMATION

Order	Wang Taxon Names	Species on Phylogen	*mirFam*	*Mkdn* (g)	*Mhrt* (g)	*Mlvr* (g)	*Mbrn* (g)	*Mcor* (g)	*Mbdy* (g)	*MRkdn* (W)	*MRhrt* (W)	*MRlvr* (W)	*MRbrn* (W)	*MRcor* (W)	*MRbdy* (W)
Primates	*Alouatta sara*	*Alouatta palliata*	174	9.90	24.00	81.20	56.50	171.60	4399.60	13.7088	13.6112	33.6452	12.9948	73.9600	169.5872
Primates		*Callithrix jacchus*	172	2.90	2.80	17.80	7.30	30.80	311.80	6.0390	17.9280	37.3520	20.4530	81.7720	180.7072
Primates	*Cebualla pygmaea*	*Callithrix pygmaea*	171	1.90	0.86	13.50	4.40	20.66	162.66	6.8432	11.1622	29.0377	20.9296	67.9727	112.3625
Primates		*Cheirogaleus medius*	176	1.00	0.93	6.30	2.80	11.03	231.03	1.5238	0.9486	15.0120	2.5432	20.0276	25.7786
Primates		*Chlorocebus pygeryt*	199	12.10	42.60	89.00	80.80	224.50	5300.50	2.2040	2.8616	16.6430	3.8471	25.5557	35.7841
Primates		*Colobus guereza*	198	23.30	37.00	171.00	86.50	317.80	9749.80	2.9356	3.5644	14.5530	6.2832	27.3362	46.7808
Primates		*Eulemur fulvus*	180	9.50	11.80	43.40	22.50	87.20	2500.20	1.4364	3.3495	13.2480	4.0794	22.1133	33.0213
Primates		*Eulemur macaco*	180	14.20	9.10	77.80	24.20	125.30	1875.30	2.2227	3.4817	16.2184	4.7800	26.7028	45.6892
Primates	Human	*Homo sapiens*	208	250.00	320.00	1700.00	1300.00	3570.00	59970.00	9.2862	14.1312	40.0500	25.5600	89.0274	199.0161
Primates	*Hylobates concolor*	*Hylobates pileatus*	195	35.20	58.20	293.00	137.80	524.20	6550.20	13.3043	25.1600	63.6120	27.9395	130.0158	323.3718
Primates		*Lemur catta*	178	11.20	11.70	72.90	22.80	118.60	2074.60	12.7890	17.1350	50.2700	15.1620	95.3560	195.6392
Primates		*Leontopithecus chry*	173	4.10	3.80	18.90	13.20	40.00	642.00	27.4000	39.1620	78.5660	35.5180	180.6460	471.7060
Primates	*Macaca nigra*	*Macaca arctoides*	205	50.00	61.00	241.00	118.00	470.00	15870.00	42.6393	63.2420	115.6400	49.5900	271.1113	669.3613
Primates	Monkey	*Macaca fascicularis*	207	21.00	23.00	110.00	42.00	196.00	4500.00	21.3940	51.5696	84.2520	44.5244	201.7400	419.9400
Primates		*Mandrillus sphinx*	194	49.90	76.00	331.00	168.00	624.90	23024.90	0.8932	1.3127	3.9304	2.0060	8.1423	13.6203
Primates		*Papio hamadryas*	197	80.30	103.00	392.00	174.00	749.30	23249.30	2.2290	2.4725	9.2769	3.8025	17.7809	31.2792
Primates	*Saguinas lagonotus*	*Saguinus midas*	170	1.90	3.30	14.40	7.80	27.40	330.40	0.2841	0.2094	2.2764	0.5683	3.3382	4.4702
Primates		*Saguinus oedipus*	172	3.10	3.70	20.90	10.00	37.70	623.70	0.2342	0.1456	1.3983	0.2828	2.0609	2.9009
Primates		*Saimiri boliviensis*	174	6.70	6.50	19.40	29.00	61.60	1002.60	0.6090	0.3464	3.7466	0.7304	5.4324	8.1513
Primates		*Sapajus apella*	171	10.40	13.40	49.30	50.80	123.90	1749.90	0.5126	0.2592	3.4181	0.2913	4.4812	5.7940
Primates		*Symphalangus synda*	194	43.70	51.50	294.00	143.00	532.20	8500.20	1.1790	0.9318	9.5588	1.2834	12.9530	20.5774
Primates		*Theropithecus gelad*	203	38.00	77.20	236.00	140.90	492.10	11402.10	0.2741	0.1024	1.4334	0.2923	2.1023	2.9479
Primates		*Trachypithecus vetu*	197	15.40	19.20	90.00	72.00	196.60	4999.60	0.4738	0.2173	3.2058	0.3715	4.2684	5.6284
Primates		*Varecia rubra*	181	22.40	18.10	72.20	35.70	148.40	4200.40	0.2504	0.1999	2.1967	0.4497	3.0967	4.0311
Scandentia		*Tupaia glis*	151	1.10	1.17	3.40	3.40	9.07	141.07	0.3189	0.2477	1.8350	0.4606	2.8622	4.1364
Glires		*Acomys minous*	157	0.32	0.18	0.90	0.90	2.30	42.30	0.7790	0.9849	6.3756	1.5400	9.6795	18.1055
Glires		*Apodemus flavicollis*	141	0.34	0.18	1.00	0.61	2.13	25.13	7.2688	9.5589	41.0427	9.1884	67.0588	118.8928
Glires		*Apodemus sylvaticus*	155	0.26	0.14	1.10	0.57	2.07	18.07	6.0705	9.4282	23.2190	8.8200	47.5377	109.5518
Glires		*Arvicola sapidus*	149	0.70	0.28	2.60	1.10	4.68	61.68	9.3010	7.5257	44.9684	9.8736	71.6687	118.9187
Glires	Guinea Pig	*Cavia porcellus*	174	5.60	2.30	27.00	4.70	39.60	799.60	4.6230	5.7850	13.2502	12.9340	36.5922	64.7281
Glires		*Gerbillus perpallidus*	147	0.27	0.13	1.00	0.58	1.98	29.98	110.0000	140.8000	340.0000	312.0000	902.8000	1489.3600
Glires		*Glaucomys volans*	176	0.59	0.56	2.90	1.90	5.95	54.95	20.7680	41.4966	121.3020	47.1276	230.6942	362.6636
Glires		*Glis glis*	168	0.68	0.48	3.20	1.50	5.86	83.86	25.2149	35.5865	113.4840	47.0470	221.3324	388.6604
Glires		*Jaculus jaculus*	158	0.29	0.45	1.10	1.20	3.04	48.04	7.2600	31.1406	38.9820	28.4416	105.8242	221.0494
Glires		*Lepus europaeus*	173	18.50	28.90	90.40	14.80	152.60	3338.60	26.4969	46.7400	97.6450	48.0480	218.9299	617.6499
Glires		*Microtus agrestis*	148	0.17	0.12	0.63	0.39	1.31	15.31	11.5440	22.3108	44.7480	5.5648	84.1676	162.2246
Glires		*Microtus arvalis*	153	0.55	0.19	1.90	0.39	3.03	27.03	4.3533	4.2864	22.0480	3.5392	34.2269	61.9490
Glires		*Microtus pinetorum*	154	0.36	0.15	1.10	0.58	2.19	21.19	0.5766	0.5731	4.2560	0.9540	6.3598	9.8932
Glires		*Mus musculus*	167	0.28	0.07	0.68	0.36	1.39	15.39	0.6747	0.7676	3.6366	1.4784	6.5573	10.7962
Glires	Mouse	*Mus_Musculus dome*	167	0.51	0.16	1.80	0.50	2.97	27.97	0.5180	0.7022	4.3094	1.2825	6.8122	9.1936
Glires		*Myodes glareolus*	143	0.24	0.10	0.67	0.35	1.36	15.36	1.3056	1.7629	5.3185	3.3831	11.7701	21.4049
Glires		*Octodon degus*	156	1.10	0.41	4.80	1.90	8.21	129.21	2.3040	2.6488	12.8904	3.6075	21.4507	39.9589
Glires		*Peromyscus leucopu*	160	0.30	0.15	1.20	0.74	2.39	22.39	0.8998	0.4649	5.6736	1.1343	8.1726	13.2667
Glires		*Rattus norvegicus*	168	1.50	0.87	9.20	2.30	13.87	209.87	3.9368	2.1022	19.6020	2.1667	27.8077	51.4437
Glires	Rat	*Rattus rattus*	167	2.80	1.10	14.30	1.90	20.10	390.10	0.2575	0.5738	1.6973	0.8256	3.3542	5.5907
Glires		*Rhabdomys pumilio*	161	0.41	0.21	1.80	0.60	3.02	50.02	0.2870	0.2327	1.4337	0.6300	2.5835	4.6115
Glires		*Sciurus carolinensis*	175	3.20	2.80	16.40	7.50	29.90	595.90	0.3427	0.2108	2.1175	0.4489	3.1199	4.2048
Glires		*Sciurus niger*	165	3.00	2.50	10.70	7.50	23.70	412.70	0.1659	0.1747	1.3148	0.3151	1.9706	2.8106
Glires		*Sciurus vulgaris*	175	1.70	1.70	5.50	6.30	15.20	274.20	0.2495	0.1751	1.7480	0.4263	2.5989	4.1025
Glires		*Sylvilagus floridanus*	170	6.30	4.80	32.00	7.90	51.00	972.00	2.0888	1.0945	12.5840	0.9709	16.7382	29.7252
Glires		*Tamias striatus*	173	0.81	0.66	2.90	2.40	6.77	103.77	0.3629	0.2661	2.7414	0.4098	3.7801	6.0972

Table S1. Summary of *mirFam*, mass and resting metabolic rates for organs, core and body. All physiological data were obtained from Wang et al (2012), most of which were compiled by Navarette et al (2011). The names of the indicated taxa were substituted with congeneric species on the phylogenies of Álvarez-Carretero et al (2022) and Shao et al (2023).

Order	Species	*mirFam*	ECV	Mass (g)	T_b (°C)
Catarrhini	*Homo sapiens*	208	1252.00	50000	37.0
Catarrhini	*Pan troglodytes*	206	368.35	44967	35.7
Catarrhini	*Gorilla gorilla*	202	490.41	120950	35.5
Catarrhini	*Macaca fascicularis*	207	63.98	4251	37.6
Catarrhini	*Macaca mulatta*	208	88.98	6793	37.3
Catarrhini	*Papio hamadryas*	197	146.17	14150	38.0
Catarrhini	*Chlorocebus aethiops*	199	65.00	3720	36.8
Catarrhini	*Erythrocebus patas*	201	97.73	9450	39.3
Catarrhini	*Cercopithecus mitis*	200	71.33	6109	37.5
Catarrhini	*Colobus guereza*	198	74.39	8589	37.0
Platyrrhini	*Callithrix jacchus*	172	7.24	320	36.0
Platyrrhini	*Callithrix pygmaea*	171	4.17	116	35.2
Platyrrhini	*Aotus trivirgatus*	177	16.85	989	38.0
Platyrrhini	*Saimiri sciureus*	174	24.14	799	38.0
Platyrrhini	*Alouata palliata*	174	49.88	6250	36.0
Lemuriformes	*Eulemur fulvus*	180	25.77	2292	36.5
Lemuriformes	*Cheirogaleus medius*	176	2.60	140	38.0
Lemuriformes	*Propithecus verreauxi*	180	26.21	2955	36.0
Lorisiformes	*Otolemur garnettii*	166	11.50	764	36.0
Lorisiformes	*Otolemur crassicaudatus*	166	11.78	1150	36.6
Lorisiformes	*Galago senegalensis*	165	3.96	194	37.9
Lorisiformes	*Loris tardigradus*	166	5.87	193	35.5
Lorisiformes	*Nycticebus coucang*	167	10.13	653	35.4
Lorisiformes	*Arctocebus calabarensis*	166	6.92	309	36.0
Lorisiformes	*Perodicticus potto*	169	12.42	835	35.4

Table S2. Summary of *mirFam*, brain volume (ECV), body mass and temperature for 25 primates. Endocranial volume (ECV) and body mass were obtained from Grabowski et al, 2023. Temperatures were obtained from the AnAge database (Magalhães et al, 2024).

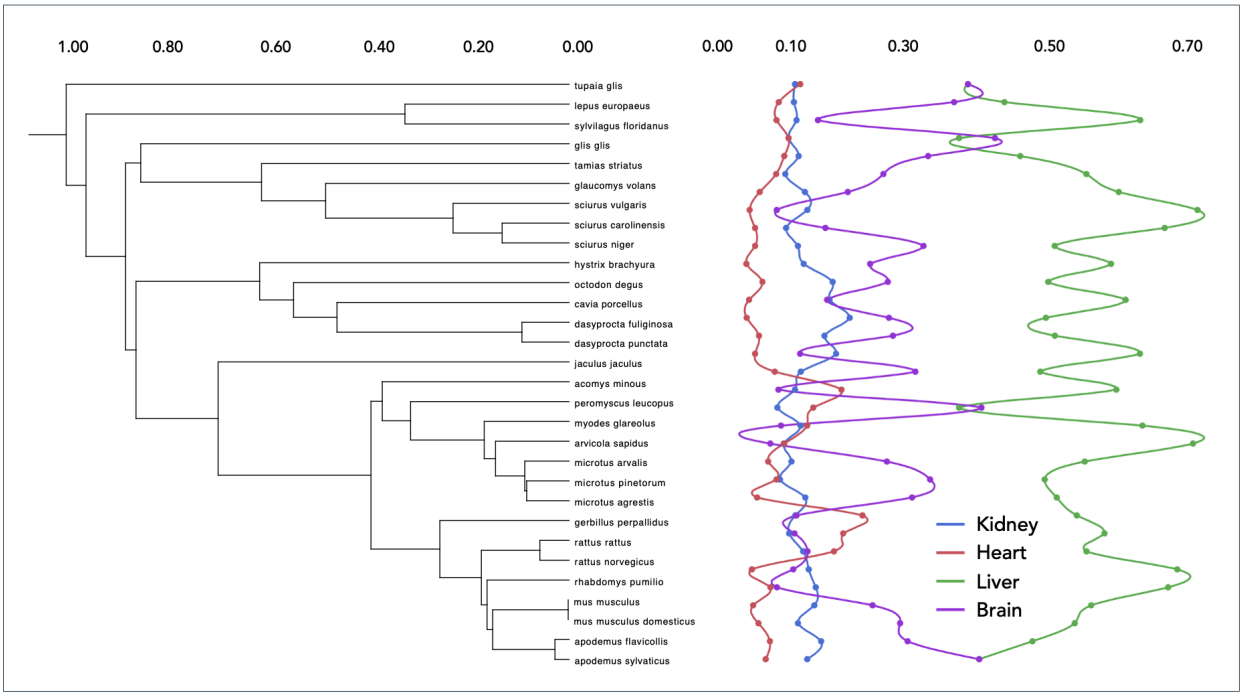

Figure S1. The proportions of brain and liver vary reciprocally in a 4-organ core.
Species include one Scandentia, two Lagomorpha, and 27 Glires, including three Sciuridae.

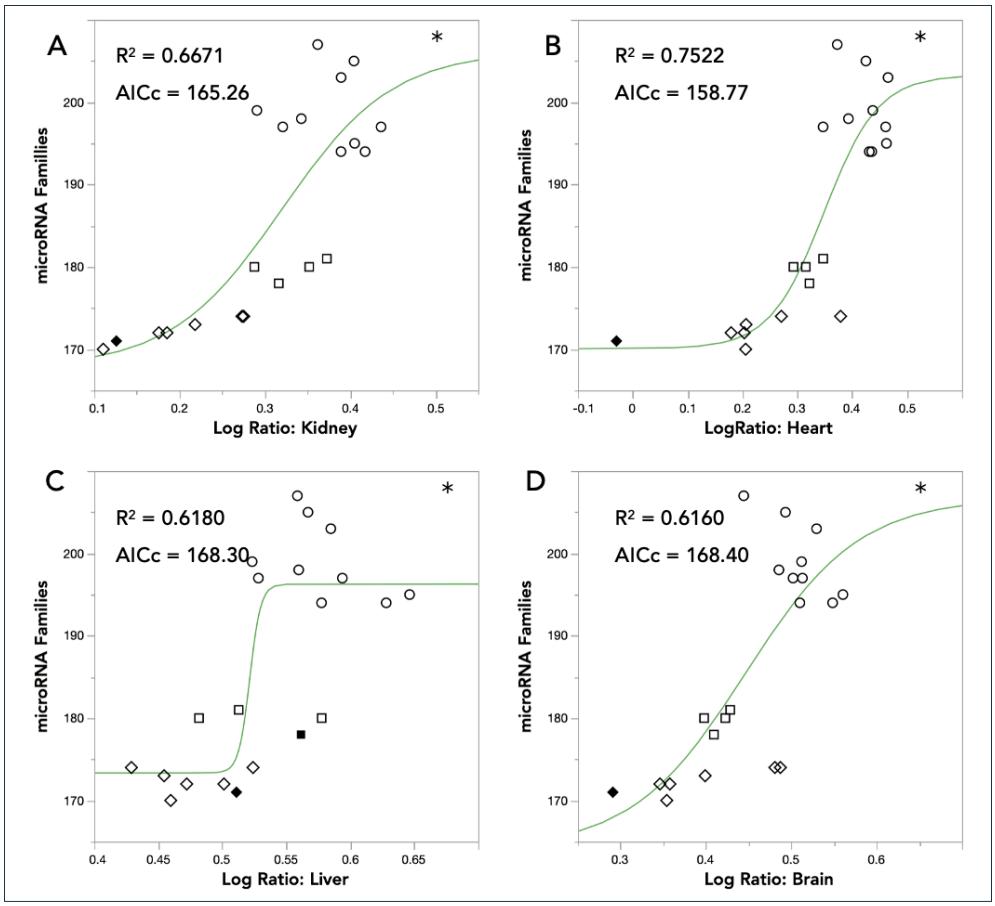

Figure S2. Logistic models for the size evolution of four thermogenic organs.
Symbols representing clades as in previous figures, with shaded symbols representing heterotherms.

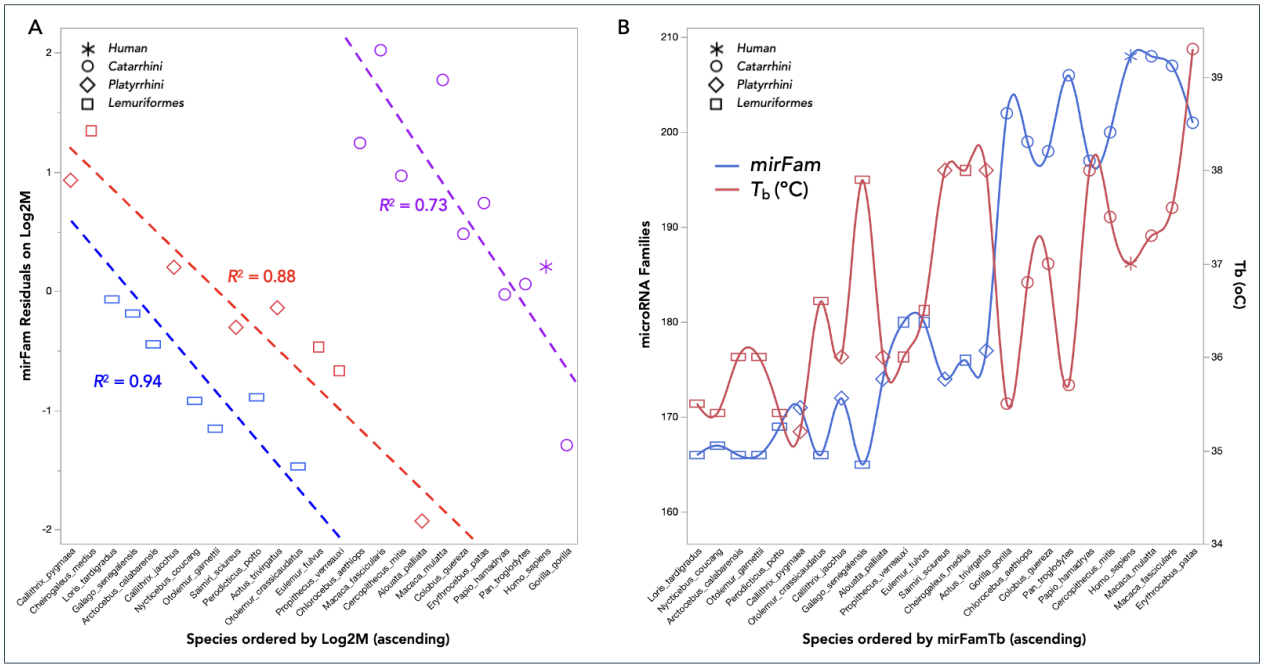

Figure S3. Conservation of *mirFam* x T_b and its relation to body size.
A.Regardless of clade, the largest species deviate the least from the *mirFam*-$\log_2 M$ relationship.
B.Visualization of the reciprocal variation of *mirFam* and T_b.

	Allometric Exponent	Pagel's *lambda*	R^2	*P*	*AICc*
KIDNEY	0.80	0	0.5366	6.39E-05	-42.7
	0.75	0	0.5834	2.14E-05	-20.09
	0.70	0	0.5958	1.56E-05	-0.93
	0.65	0	0.5946	1.61E-05	16.22
	0.60	0	0.5859	2.00E-05	32.13
		Pagel's *lambda*	R^2	*P*	*AICc*
HEART	0.80	0	0.4937	1.60E-04	-38.02
	0.75	0	0.6476	3.83E-06	-17.88
	0.70	0	0.6962	8.44E-07	0.63
	0.65	0	0.7133	4.69E-07	17.65
	0.60	0	0.7163	4.21E-07	33.66
		Pagel's *lambda*	R^2	*P*	*AICc*
LIVER	0.80	0	0.5724	2.79E-05	-15.22
	0.75	0	0.4011	9.28E-04	-10.98
	0.70	0	0.0854	1.01E-01	-2.86
	0.65	0	-0.0344	5.89E-01	10.24
	0.60	0.962	0.0145	2.66E-01	27.34
		Pagel's *lambda*	R^2	*P*	*AICc*
BRAIN	0.80	1	0.0329	2.05E-01	-63.9
	0.75	1	0.107	7.55E-02	-35.75
	0.70	1	0.1336	5.07E-02	-10.58
	0.65	1	0.151	4.17E-02	11.76
	0.60	1	0.1596	3.71E-02	32.24

Supplementary Table S3. Summary of phylogenetic regressions of organ *cMR*s on *mirFam*.